Article:
Deane, O.J., Musa, O.M., Fernyhough, A. et al. (2020) Synthesis and characterization of waterborne pyrrolidone-functional diblock copolymer nanoparticles prepared via surfactant-free RAFT emulsion polymerization. Macromolecules, 53 (4). pp. 1422-1434. ISSN: 0024-9297

https://doi.org/10.1021/acs.macromol.9b02394

Synthesis and Characterization of Waterborne Pyrrolidone-functional Diblock Copolymer Nanoparticles Prepared *via* Surfactant-free RAFT Emulsion Polymerization

Oliver J. Deane[a], Osama M. Musa[b], Alan Fernyhough[c] and Steven P. Armes[a,*]

a. Dainton Building, Department of Chemistry, University of Sheffield, Brook Hill, Sheffield, South Yorkshire, S3 7HF, UK.

b. Ashland Specialty Ingredients, 1005 US 202/206, Bridgewater, New Jersey, 08807, USA.

c. Ashland Specialty Ingredients, Listers Mills, Heaton Road, Bradford, West Yorkshire, BD9 4SH, UK.

Abstract. Polymerization-induced self-assembly (PISA) enables the facile synthesis of a wide range of block copolymer nano-objects in the form of concentrated dispersions. In this context, many surfactant-free reversible addition-fragmentation chain transfer (RAFT) aqueous emulsion polymerization formulations have been reported using various non-ionic and polyelectrolytic water-soluble precursors for the steric stabilizer block. In the present study, we examine poly(2-(*N*-acryloyloxy)ethyl pyrrolidone) (PNAEP) as a new non-ionic stabilizer block. A trithiocarbonate-based PNAEP precursor with a mean degree of polymerization of 67 was employed as the steric stabilizer for the RAFT emulsion polymerization of styrene, *n*-butyl acrylate (nBA) or statistical mixtures thereof. RAFT emulsion polymerization of styrene using a VA-044 azo initiator at 80 °C and pH 7 led to essentially full conversion within 40 min with induction times as short as 10 min, while GPC analysis confirmed efficient chain extension and relatively low dispersities (M_w/M_n < 1.30). Dynamic light scattering (DLS) studies indicated that systematically increasing the target DP from 100 to 700 enabled the z-average diameter of the resulting kinetically-trapped spherical nanoparticles to be varied from

55 to 156 nm. The same $PNAEP_{67}$ precursor was then employed for the RAFT emulsion polymerization of nBA at 30 °C using a low-temperature redox initiator at pH 3. More than 99% conversion was achieved within 25 min and efficient chain extension was observed up to a PnBA target DP of 700. However, relatively broad MWDs (M_w/M_n = 1.38-1.64) were obtained, presumably owing to side-reactions such as chain transfer to polymer. DLS studies indicated that a series of kinetically-trapped $PNAEP_{67}$-$PnBA_x$ spheres (where x = 100 to 700) exhibited z-average diameters ranging from 45 to 141 nm. Attempts to use this low-temperature initiator protocol for the homopolymerization of styrene led to essentially no conversion after 48 h at 30 °C. However, the statistical copolymerization of 45% styrene with 55% nBA could be achieved using this low-temperature redox initiator at 30 °C using the same $PNAEP_{67}$ precursor. In this case, ^{1}H NMR studies indicated a significantly longer induction period (95 min) compared to either homopolymerization. Nevertheless, once the copolymerization commenced, essentially full conversion of both comonomers could be achieved within 45 min. Differential scanning calorimetry analysis indicated that these statistical copolymers exhibited intermediate glass transition temperatures compared to the two respective homopolymers. The film formation behavior of selected diblock copolymer nanoparticles was briefly explored.

Author to whom correspondence should be addressed (s.p.armes@shef.ac.uk)

Introduction

The development of controlled/living radical polymerization for vinyl monomers over the past twenty-five years or so has enabled the synthesis of many examples of functional amphiphilic block copolymers with pre-determined molecular weights and narrow molecular weight distributions (M_w/M_n < 1.30).[1-3] More recently, polymerization-induced self-assembly (PISA) has allowed the convenient preparation of a wide range of block copolymer nano-objects directly in the form of

concentrated dispersions.[4] During PISA, a soluble homopolymer precursor is chain-extended in a suitable solvent such that the growing second block becomes insoluble at some critical chain length. This drives *in situ* self-assembly to produce sterically-stabilized spheres of tunable size. Depending on the precise PISA formulation, other morphologies such as worms, vesicles or lamellae can be obtained.[5-16] PISA is much more scalable than traditional post-polymerization processing routes, because the latter are multi-step processes involving organic co-solvents and typically conducted in dilute solution.[15, 17-20] Various living polymerization chemistries can be used for PISA, including reversible addition-fragmentation chain transfer (RAFT) polymerization,[21-24] atom transfer radical polymerization (ATRP)[25] and nitroxide-mediated polymerization (NMP).[26] To date, the majority of PISA syntheses have been conducted using RAFT polymerization.[27-36] Such radical-based polymerizations are tolerant of a wide range of monomer functionality and can be performed in both non-polar solvents[37] and polar solvents,[11, 38, 39] including water.[36, 40, 41]

In principle, RAFT aqueous emulsion polymerization combines the advantages of traditional emulsion polymerization (fast polymerization rates, high final monomer conversions, low solution viscosities and a cost-effective, environmentally-friendly solvent) with good control over the molecular weight distribution (MWD) and convenient introduction of functional end-groups.[42-49] Moreover, the covalent bond between the stabilizer and core-forming blocks leads to more effective and efficient stabilization compared to that achieved for surfactant-stabilized latexes prepared by conventional emulsion polymerization.[50] In principle, such surfactant-free protocols should enable copolymer films to be prepared with superior transparency.[51] Anionic steric stabilizer blocks such as poly(methacrylic acid) or poly(acrylic acid) have been employed for various RAFT aqueous emulsion polymerization formulations.[52-54] However, their polyelectrolytic character produces nanoparticles with pH-dependent colloidal stability.[55] In principle, using non-ionic stabilizer blocks such as poly(ethylene glycol) or poly(glycerol monomethacrylate) eliminates this problem.[56-61] However, there are relatively few other examples of *non-ionic* stabilizer blocks in the aqueous PISA literature.[62, 63] According to Lansalot and Rieger, increasing the scope of RAFT emulsion polymerization is expected to aid the

development of commercially-relevant PISA protocols.[8] This deficiency is addressed in the current study.

Poly(*N*-vinylpyrrolidone) (PNVP) is a highly polar, non-ionic water-soluble polymer. It can be readily prepared by conventional radical polymerization and its excellent biocompatibility, strong binding capacity and good film-forming ability has led to a wide range of commercial applications.[64, 65] For example, PNVP is used as an excipient for pharmaceutical formulations, as an anti-dye transfer agent for laundry products, and as a film-forming agent for hair sprays and other cosmetics.[66-69] PNVP-based diblock copolymers can be prepared by macromolecular design *via* the interchange of xanthates (MADIX, which is a type of RAFT polymerization).[70-73] However, NVP is known to undergo undesirable side-reactions in aqueous media, leading to poor RAFT control and incomplete conversions.[74-76] As far as we are aware, there are only two reported examples of the use of PNVP as a stabilizer block for RAFT aqueous emulsion polymerization.[10, 77] Binaud *et al*. prepared PNVP-stabilized nanoparticles via RAFT aqueous emulsion polymerization of vinyl acetate (VAc). However, monomer conversions remained below 90% and the resulting PNVP-PVAc diblock copolymers had rather broad MWDs ($M_w/M_n > 2.0$) as determined by gel permeation chromatography (GPC). Furthermore, a relatively high proportion of PNVP stabilizer chains remained unreacted at the end of the polymerization, leading to a bimodal MWD. In principle, (meth)acrylic analogues of NVP should provide much better copolymerizability with a wide range of vinyl monomers, enabling the optimized PISA synthesis of well-defined pyrrolidone-based diblock copolymer nanoparticles in the form of concentrated aqueous dispersions.

For example, Cunningham *et al.* polymerized 2-(*N*-methacryloyloxy)ethylpyrrolidone (NMEP) with good control in PISA syntheses conducted in both alcoholic[78] and non-polar[79] solvents. However, PNMEP homopolymer is significantly less hydrophilic than PNVP and exhibits lower critical solution temperature (LCST) behavior. Indeed, this property was exploited to prepare PNMEP-core diblock copolymer nanoparticles *via* RAFT aqueous dispersion polymerization.[80] Recently, Gibson *et al*.

prepared a series of PNMEP stabilizers with anionic carboxylate end-groups using an appropriate RAFT agent.[81] This minor modification was sufficient to eliminate the undesirable LCST behavior and hence enable the synthesis of well-defined diblock copolymer spheres *via* aqueous PISA at pH 7 using PNMEP as an electrosteric stabilizer.[81] However, such nanoparticles became flocculated in the presence of relatively low levels of added salt. In principle, this colloidal instability problem can be addressed by replacing NMEP with 2-(*N*-(acryloyloxy)ethylpyrrolidone (NAEP), which is significantly more hydrophilic.[82] In this context, Deane *et al*. recently reported that a series of well-defined low-dispersity PNAEP homopolymers can be readily prepared by RAFT aqueous solution polymerization, with monomer conversions of more than 99% being achieved at reaction temperatures ranging from 30 to 70 °C.[83] Turbidimetry studies confirmed that such PNAEP homopolymers did not exhibit LCST behavior, while differential scanning calorimetry (DSC) experiments indicated relatively low glass transition temperatures (T_g) of between 10 and 20 °C. A range of PNAEP-based stimulus-responsive diblock copolymers were prepared *via* RAFT aqueous solution polymerization, with micellar self-assembly being observed on varying the solution pH or temperature.

Herein we report the synthesis of well-defined PNAEP-based diblock copolymer spheres *via* RAFT emulsion polymerization of styrene, *n*-butyl acrylate or statistical mixtures thereof. Polystyrene is a model high T_g polymer that has been well-studied in the context of PISA.[46, 49, 53, 55, 63, 84-86] Polystyrene-based nanoparticles are straightforward to image by transmission electron microscopy (TEM), which aids morphological assignments. In contrast, poly(*n*-butyl acrylate) has a relatively low Tg (–54 °C) and can be considered to be a model film-forming polymer.[58, 87, 88] Statistical copolymers based to these two comonomers enable the T_g to be tuned over a wide range, which is convenient for paints and coatings applications.[43, 89, 90] ^{1}H NMR spectroscopy was used to study the kinetics of the optimized RAFT emulsion polymerization, while chloroform GPC was used to assess the evolution in the molecular weight distribution. Differential scanning calorimetry was used to determine T_g values for the resulting diblock copolymers. Finally, the film formation behavior of selected diblock copolymer nanoparticles was briefly explored by visible adsorption spectroscopy.

Experimental

Materials. 2-(*N*-Acryloyloxy)ethyl pyrrolidone (NAEP; 95%) was kindly provided by Ashland Specialty Ingredients (Cherry Hill, NJ, USA) and was purified by dilution with chloroform followed by sequential washes with 5% Na_2CO_3 solution, saturated NaCl solution, and finally deionized water. This solution was then dried over anhydrous $MgSO_4$ prior to use. All chemicals used for NAEP purification were purchased from Sigma-Aldrich (Dorset, UK) and were used as received. Styrene (S), ascorbic acid (AsAc), potassium persulfate (KPS), 2-(dodecylthiocarbonothioylthio)-2- methylpropionic acid (DDMAT; 98%) and *n*-butyl acrylate (nBA) were purchased from Sigma-Aldrich (Dorset, UK). 2,2-Azobis[2-(2-imidazolin-2-yl)propane]dihydrochloride (VA-044) was purchased from Wako and used without further purification. $CDCl_3$ was purchased from Goss Scientific Instruments Ltd. (Cheshire, UK). All other solvents were purchased from Fisher Scientific (Loughborough, UK) and were used as received. Deionized water was used for all experiments.

Preparation of $PNAEP_{67}$ Macro-CTA. The synthesis of PNAEP precursors by RAFT aqueous solution polymerization has been previously reported[83]: NAEP (10.00 g, 54.6 mmol), DDMAT RAFT agent (199.0 mg, 0.546 mmol; target DP = 100), and AsAc (1.0 mg, 5.5 µmol) were weighed into a 14 mL vial charged with a magnetic flea (reaction solution 1). This reaction solution was then placed in an ice bath and degassed with nitrogen for 30 min. Deionized water (4.372 g, 70% w/w) and KPS (1.5 mg, 5.5 µmol; DDMAT/KPS molar ratio = 100) were weighed into a second 14 mL vial (reaction solution 2) and degassed with nitrogen in an ice bath for 30 min. After 30 min, the vial containing reaction solution 1 was immersed in an oil bath set at 30 °C. Reaction solution 2 was then added using a degassed syringe and needle to reaction solution 1 under nitrogen. The NAEP polymerization was allowed to proceed for 8 min before being quenched *via* exposure to air and immersed in an ice bath. ^{1}H NMR analysis of the disappearance of vinyl signals at 5.9 and 6.4 ppm relative to the integrated four ethyl protons at 3.4−3.8 ppm assigned to PNAEP indicated a monomer conversion of 62%. The crude PNAEP homopolymer was purified by dialysis against water (72 h) using a 3500 MWCO dialysis membrane

(Fisher Scientific) to give a PNAEP macro-CTA containing less than 1% residual monomer. Its mean DP was calculated to be 67 as judged by ^{1}H NMR spectroscopy analysis in $CDCl_3$ (comparison of the integral at 3.4-3.8 ppm (m, 4H) with that assigned to the methyl RAFT chain-end at 0.86-0.96 ppm (t, 3H)). Chloroform GPC analysis indicated an M_n of 19.2 kg mol^{-1} and an M_w/M_n of 1.19.

Synthesis of PNAEP$_{67}$-PS$_x$ Diblock Copolymers via RAFT Aqueous Emulsion Polymerization of Styrene at 80 °C. A typical protocol used for the synthesis of the PNAEP$_{67}$–PS$_{350}$ diblock copolymer was as follows: PNAEP$_{67}$ macro-CTA (0.185 g, 14.6 µmol), deionized water (2.880 g, corresponding to a 20% w/w solution) and VA-044 (1.580 mg, 4.9 µmol; PNAEP$_{67}$/VA-044 = 3.0) were weighed into a 10 mL round-bottom flask charged with a magnetic flea. NaOH (20 µL, 1 M) was added to raise the pH to 7.0. This flask was then immersed in an ice bath and the solution was degassed with nitrogen for 30 min. Styrene (1.0 g) was weighed into a separate 14 mL vial and degassed with nitrogen in an ice bath for 30 min. After 30 min, styrene (0.59 ml, 5.12 mmol; target DP = 350) was added to the flask using a degassed syringe and needle under nitrogen. The contents of the flask were then stirred vigorously to ensure thorough mixing and degassed for a further 5 min before being immersed in an oil bath set at 80°C. The styrene polymerization was allowed to proceed for 2 h before being quenched by exposing the reaction solution to air and immersing the reaction vial in an ice bath. ^{1}H NMR spectroscopy analysis of the disappearance of vinyl signals at 5.3 and 5.8 ppm (relative to the integrated five aromatic protons at 6.3–7.2 ppm assigned to PS) indicated a final styrene conversion of 99%. Chloroform GPC analysis indicated a M_n of 46.6 kg mol^{-1} and an M_w/M_n of 1.28. Other target diblock copolymer compositions were obtained by adjusting the styrene/PNAEP$_{67}$ molar ratio.

Synthesis of PNAEP$_{67}$-PnBA$_x$ Diblock Copolymer Nanoparticles via RAFT Aqueous Emulsion Polymerization of n-Butyl Acrylate at 30 °C. A typical protocol used for the synthesis of the PNAEP$_{67}$–PnBA$_{500}$ diblock copolymer was as follows: PNAEP$_{67}$ macro-CTA (0.185 g, 14.6 µmol), deionized water (4.501 g, corresponding to a 20% w/w solution) and KPS (1.320 mg, 4.9 µmol; PNAEP$_{67}$/KPS = 3.0) were weighed into a 10 mL round-bottom flask charged with a magnetic flea. HCl

(10 µL, 0.2 M) was added to reduce the pH to 3.0. This flask was then immersed in an ice bath, and the solution was degassed with nitrogen for 30 min. nBA (1.500 g) was weighed into a separate 14 mL vial and degassed with nitrogen in an ice bath for 30 min. An AsAc stock solution (0.01% w/w) was weighed into a second 14 mL vial and degassed with nitrogen in an ice bath for 30 min. After 30 min nBA (1.05 ml, 7.32 mmol; target DP = 500) was added to the flask using a degassed syringe and needle under nitrogen. The flask contents were then stirred vigorously to ensure thorough mixing and degassed for 5 min before being immersed in an oil bath set at 30°C. After 1 min, AsAc (0.09 ml, 4.9 µmol; KPS/AsAc molar ratio = 1.0) was added to the flask. The nBA polymerization was allowed to proceed for 1 h before being quenched by exposing the reaction solution to air and immersing the reaction vial in an ice bath. ^{1}H NMR spectroscopy analysis of the disappearance of vinyl signals at 5.8 and 6.1 ppm (relative to the integrated three protons at 0.9−1.0 ppm assigned to the pendant methyl group of PnBA) indicated a final nBA conversion of 99%. Chloroform GPC analysis of this copolymer indicated a M_n of 86.6 kg mol^{-1} and an M_w/M_n of 1.56. Other diblock copolymer compositions were obtained by adjusting the nBA/PNAEP$_{67}$ molar ratio.

Synthesis of PNAEP$_{67}$-P(S-stat-nBA)$_x$ Diblock Copolymer Nanoparticles via RAFT Aqueous Emulsion Polymerization of n-Butyl Acrylate at 30 °C. A typical protocol used for the synthesis of the PNAEP$_{67}$−P(S-*stat*-nBA)$_{400}$ diblock copolymer was as follows: PNAEP$_{67}$ macro-CTA (0.185 g, 14.6 µmol), deionized water (3.472 g, corresponding to a 20% w/w solution) and KPS (1.320 mg, 4.9 µmol; PNAEP$_{67}$/KPS = 3.0) were weighed into a 10 mL round-bottom flask charged with a magnetic flea. HCl (10 µL, 0.2 M) was added to reduce the pH to 3.0. This flask was then immersed in an ice bath, and the solution was degassed with nitrogen for 30 min. nBA and styrene (1.500 g) were weighed into separate 14 mL vials and degassed with nitrogen in an ice bath for 30 min. An AsAc stock solution (0.01% w/w) was weighed into a second 14 mL vial and degassed with nitrogen in an ice bath for 30 min. After 30 min styrene (0.34 ml, 2.97 mmol) and nBA (0.41 ml, 2.89 mmol; overall copolymer DP = 400, nBA content = 55 % by mass) was added to the flask using a degassed syringe and needle under nitrogen. The flask contents were then stirred vigorously to ensure thorough mixing and degassed for

5 min before being immersed in an oil bath set at 30°C. After 1 min, AsAc (0.09 ml, 4.9 µmol; KPS/AsAc molar ratio = 1.0) was added to the flask. The polymerization was allowed to proceed for 3 h before being quenched by exposing the reaction solution to air and immersing the reaction vial in an ice bath. ^{1}H NMR spectroscopy analysis of the disappearance of vinyl signals at 5.8 and 6.1 ppm (relative to the integrated three protons at 0.8−1.0 ppm assigned to the pendant methyl group of PnBA) and the vinyl signals at 5.3 and 5.8 ppm (relative to the integrated five aromatic protons at 6.5–7.2 ppm assigned to PS) indicated a final comonomer conversion of 99% conversion. Chloroform GPC analysis of this copolymer indicated a M_n of 86.6 kg mol^{-1} and an M_w/M_n of 1.56. Other diblock copolymer compositions were obtained by adjusting the (styrene+nBA)/PNAEP$_{67}$ molar ratio.

^{1}H NMR Spectroscopy. All ^{1}H NMR spectra were recorded in $CDCl_3$ using a 400 MHz Bruker Avance-400 spectrometer with 64 scans being averaged per spectrum. Anhydrous $MgSO_4$ was used as a desiccant to remove water and hence enable molecular dissolution of each diblock copolymer.

Gel Permeation Chromatography (GPC). Copolymer molecular weights and dispersities were determined using an Agilent 1260 Infinity GPC system equipped with both refractive index and UV−visible detectors. Two Agilent PL gel 5 µm Mixed-C columns and a guard column were connected in series and maintained at 35 °C. HPLC-grade chloroform containing 0.25% w/w triethylamine was used as the eluent and the flow rate was set at 1.0 mL min^{-1}. The refractive index detector was used for calculation of molecular weights and dispersities by calibration using a series of ten near-monodisperse polystyrene standards (with M_n values ranging from 370 to 2,520,000 g mol^{-1}).

Transmission Electron Microscopy (TEM). As-prepared 20% w/w copolymer dispersions were diluted at 20 °C to generate 0.10% w/w aqueous dispersions. Copper/palladium TEM grids (Agar Scientific, UK) were coated in-house to produce thin films of amorphous carbon. These grids were then treated with a plasma glow discharge for 30 s to create a hydrophilic surface. One droplet of aqueous diblock copolymer dispersion (20 µL; 0.10% w/w) was placed on a freshly-treated grid for 1 min and then blotted with filter paper to remove excess solution. To stain the deposited nanoparticles, an aqueous

solution of uranyl formate (10 µL; 0.75% w/w) was placed on the sample-loaded grid *via* micropipet for 20 s and then carefully blotted to remove excess stain. Each grid was then dried using a vacuum hose. Imaging was performed using a Philips CM100 instrument operating at 100 kV and equipped with a Gatan 1 k CCD camera.

Dynamic Light Scattering (DLS). Measurements were conducted at 25 °C using a Malvern Instruments Zetasizer Nano series instrument equipped with a 4 mW He−Ne laser (λ = 633 nm) and an avalanche photodiode detector. Scattered light was detected at 173°. Copolymer dispersions were diluted to 0.10% w/w prior to analysis. Intensity-average hydrodynamic diameters were averaged over three runs and calculated using the Stokes-Einstein equation.

Differential Scanning Calorimetry (DSC). DSC studies were performed using a TA Instruments Discovery DSC instrument equipped with TZero low-mass aluminum pans and hermetically-sealed lids. Copolymers (and homopolymers) were equilibrated above their glass transition temperatures for 10 min before performing two consecutive thermal cycles at a rate of 10 °C min^{-1}. Two cycles were performed to minimize the thermal history of each sample.

Film preparation and visible absorption spectroscopy. Spin-coated copolymer films were prepared by depositing a 200 µL aliquot of a 20% w/w aqueous dispersion onto a glass slide mounted on a vacuum-free Ossila Spin Coater (initially rotating at 250 rpm, followed by rapid acceleration up to 3000 rpm for 15 min). For transmittance studies, films were prepared as described above and their transparency was assessed by visible absorption spectroscopy using a Perkin-Elmer Lambda 25 spectrometer. Spectra were recorded from 200 to 800 nm at 2 nm intervals at a scan speed of 960 nm/min. Copolymer film thicknesses were measured using a micrometre screw gauge.

Results and Discussion

A $PNAEP_{67}$ macro-CTA was synthesized *via* RAFT solution polymerization of NAEP in deionized water at 30 °C using 2-(dodecylthiocarbonothioylthio)-2-methylpropionic acid (DDMAT) as the chain

transfer agent (CTA) and 1:1 KPS/AsAc as a low-temperature redox initiator pair at a [DDMAT]/[KPS] molar ratio of 100. In principle, the relatively low initiator concentration should reduce termination during the synthesis of the PNAEP macro-CTA, thus improving the blocking efficiency for its subsequent chain extension.[11] This $PNAEP_{67}$ macro-CTA was then chain-extended *via* RAFT aqueous emulsion polymerization of styrene using VA-044 ([$PNAEP_{67}$]/[VA-044] molar ratio = 3.0) at 80 °C, see Scheme 1.

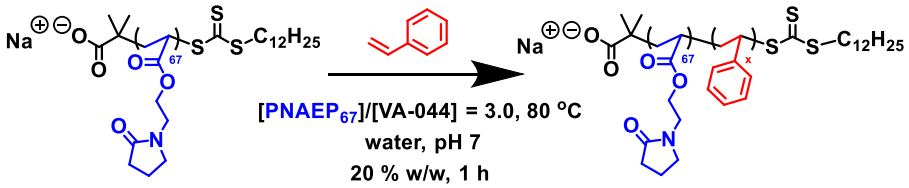

Scheme 1. Synthesis of $PNAEP_{67}$-PS_x diblock copolymer nanoparticles *via* RAFT aqueous emulsion polymerization of styrene at 80 °C using a [$PNAEP_{67}$]/[VA-044] molar ratio of 3.0.

The kinetics for the RAFT emulsion polymerization of styrene at 80 °C was monitored for a target $PNAEP_{67}$-PS_{350} diblock composition. Periodic sampling involved dilution of each aliquot extracted from the reaction mixture using $CDCl_3$, which is a good solvent for both the PNAEP and PS blocks. Anhydrous $MgSO_4$ was utilized as a desiccant to remove water in order to overcome this solvent's immiscibility with $CDCl_3$ and hence achieve molecular dissolution of the diblock copolymer chains. After quenching the polymerization *via* dilution and cooling to 20 °C, each sample was analyzed by ^{1}H NMR spectroscopy and chloroform GPC (Figure 1). The former technique indicated that more than 95% conversion was achieved within 40 min. Furthermore, the semi-logarithmic plot suggests an approximate thirty-fold increase in rate occurred between 10.0 and 12.5 min (Figure 1a), with the earlier time point corresponding to the onset of nanoparticle formation. This rate enhancement is well-known for PISA syntheses and is attributed to micellar nucleation.[6, 91, 92] This hypothesis was confirmed via DLS analysis of aliquots taken from the reaction mixture (see Figure S1a). The growing PS chains become insoluble when they reach a critical DP, which drives *in situ* self-assembly to form nascent nanoparticles. For the present PISA formulation, this critical DP is around 5, which

corresponds to just 8% conversion. Chaduc *et al.* performed the RAFT aqueous emulsion polymerization of styrene at 80 °C in the presence of a poly(acrylic acid) (PAA) macro-CTA between pH 2.5 and 7.0.[55] Empirically, the optimum solution pH was found to be pH 2.5. However, the evolution in M_n and M_w/M_n did not display the expected living character when the styrene polymerization was performed at pH 7 and induction periods of approximately 1 h were observed.[55] Moreover, a significant proportion of the initial PAA macro-CTA was consumed via hydrolysis, leading to higher than expected final M_n values.[55] In the present study, much shorter induction periods of around 10 min were observed at pH 7, which is attributed to the fact that VA-044 was employed at 80 °C. The ten-hour half-life for this initiator is only 44 °C so the radical flux is relatively high at the reaction temperature, leading to rapid polymerization even for the relatively low concentration of styrene that is dissolved in the aqueous phase (estimated to be 0.62 g dm^{-3} at 80 °C[93]). Unlike the observations made by Chaduc and co-workers, poor colloidal stability was observed for PISA syntheses conducted below pH 6. Acid titration studies indicated that the terminal carboxylic acid (-COOH) group on the PNAEP stabilizer chains has a pK_a of approximately 5.25 (see Figure S2). Thus, maintaining colloidal stability during the PISA synthesis requires a relatively high degree of ionization (>50%) of these acidic end-groups, otherwise macroscopic precipitation occurs. In this context, it is perhaps noteworthy that Gibson et al. recently reported similar observations when using carboxylic acid-functionalized PNMEP stabilizer blocks.[81] Presumably, the anionic character conferred by the carboxylate end-groups confers additional (electrosteric) colloidal stability, which is sufficient to prevent nanoparticle aggregation. Perhaps surprisingly, lowering the solution pH from pH 8.9 to pH 2.1 did not induce colloidal instability for these PNAEP-PS nanoparticles after their initial synthesis (see Figure S3).

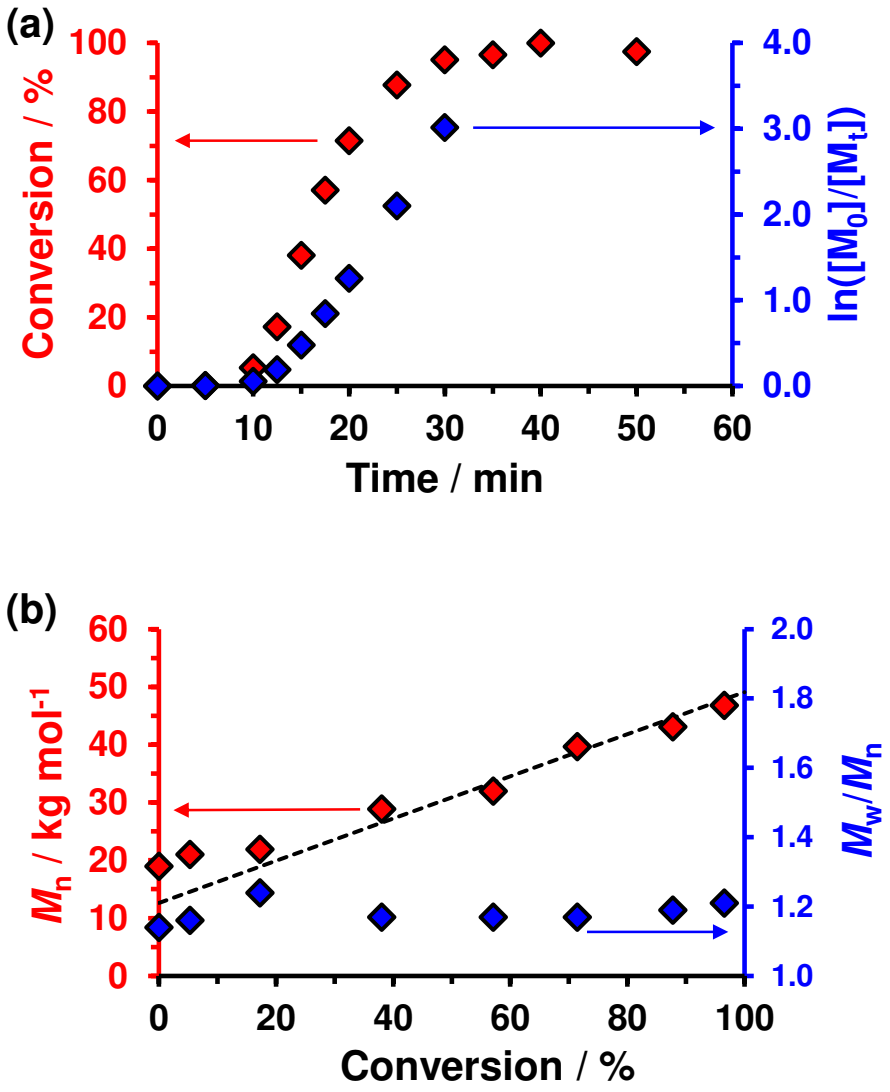

Figure 1. (a) Conversion *vs* time curve and corresponding semi-logarithmic plot determined by ^{1}H NMR spectroscopy during the RAFT aqueous emulsion polymerization of styrene at 80 °C when targeting $PNAEP_{67}$-PS_{350} diblock copolymer nanoparticles. Conditions: 20% w/w solids, [$PNAEP_{67}$]/[VA-044] molar ratio = 3.0. (b) Evolution of M_n and M_w/M_n against conversion determined by chloroform GPC using a series of near-monodisperse polystyrene calibration standards. The dashed line indicates the corresponding theoretical M_n values.

When using a [$PNAEP_{67}$]/[VA-044] molar ratio of 3.0 and targeting a polystyrene DP of 350, chloroform GPC analysis indicated a linear evolution of molecular weight with conversion. Moreover, relatively low dispersities (M_w/M_n < 1.25) were maintained throughout the reaction. Both features are

consistent with a well-controlled RAFT polymerization. However, the experimental GPC data deviate significantly from the theoretical M_n values at low conversion. This discrepancy is likely to be a systematic error incurred by the use of polystyrene standards because much better agreement was observed at higher conversions as the growing diblock copolymer chains gradually become more polystyrene-rich. Four PNAEP$_{67}$-PS$_x$ diblock copolymers were prepared by targeting polystyrene DPs ranging between 100 and 1250 while maintaining the same 20% w/w solids concentration. More than 98% styrene conversion was achieved when targeting DPs of up to 700, with relatively narrow MWDs being maintained ($M_w/M_n \leq 1.30$) (Figure 2).

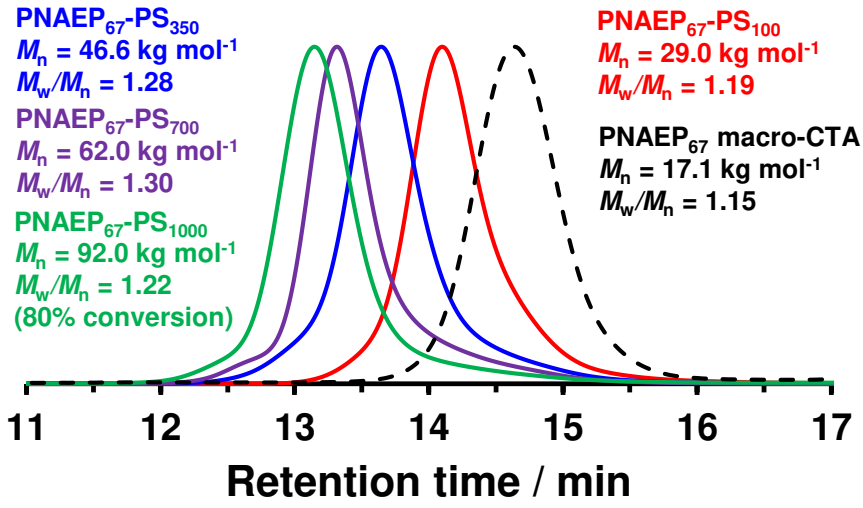

Figure 2. Chloroform GPC curves obtained for PNAEP$_{67}$-PS$_x$ diblock copolymers prepared at 20% w/w solids *via* RAFT aqueous emulsion polymerization of styrene at 80 °C (where x = 100, 350, 700 or 1000). Molecular weight data are expressed relative to a series of near-monodisperse polystyrene calibration standards. High conversions (> 98 %) were obtained when targeting PS DPs of up to 700, but only 80% conversion was achieved when targeting a PS DP of 1250 (green curve).

However, only 80% styrene conversion could be achieved when targeting a polystyrene DP of 1250. This is because such formulations require a relatively low concentration of the PNAEP$_{67}$ precursor and hence also the VA-044 initiator. Thus the radical flux is significantly lower, which in turn affects the rate of polymerization. Chloroform GPC analysis of the four PNAEP$_{67}$-PS$_x$ diblock

copolymers shown in Figure 2 confirmed relatively high blocking efficiencies for the $PNAEP_{67}$ precursor and indicated a linear evolution in M_n when targeting longer PS block DPs.

Dynamic light scattering (DLS) was used to characterize dilute aqueous dispersions of the three $PNAEP_{67}$-PS_x formulations for which 100% conversion was achieved (Figure 3). For a fixed $PNAEP_{67}$ precursor, targeting higher PS DPs proved to be a highly convenient means of controlling the overall particle size. For example, amphiphilic $PNAEP_{67}$-PS_{100} chains self-assembled to form nanoparticles with a mean hydrodynamic diameter of 55 nm, while $PNAEP_{67}$-PS_{700} formed nanoparticles of 156 nm diameter. Moreover, relatively narrow particle size distributions were obtained (PDI < 0.10). These DLS data were supported by TEM studies, which confirmed a well-defined spherical morphology in each case (Figure 3b). This suggests kinetically-trapped morphologies when targeting highly asymmetric diblock compositions such as $PNAEP_{67}$-PS_{700}.[94] Thus, the steric stabilization conferred by the $PNAEP_{67}$ stabilizer block is sufficient to prevent the stochastic 1D fusion of multiple spheres, which is a prerequisite for the production of so-called 'higher order' morphologies such as worms or vesicles.[6, 94, 95] A range of diblock copolymer compositions and copolymer concentrations were explored, but in all cases only spherical morphologies were obtained (see Figure S4). However, in at least some cases this restrictive paradigm can be overcome. For example, Hawkett and co-workers recently prepared polystyrene-based diblock copolymer vesicles via RAFT aqueous emulsion polymerization of styrene.[84] Currently, there is no convincing explanation for this rather puzzling aspect of aqueous PISA formulations, although incorporating oligo(ethylene glycol) (meth)acrylate comonomers does seem to be a useful, if rather empirical, approach for accessing worms and vesicles.[46, 54, 86, 96]

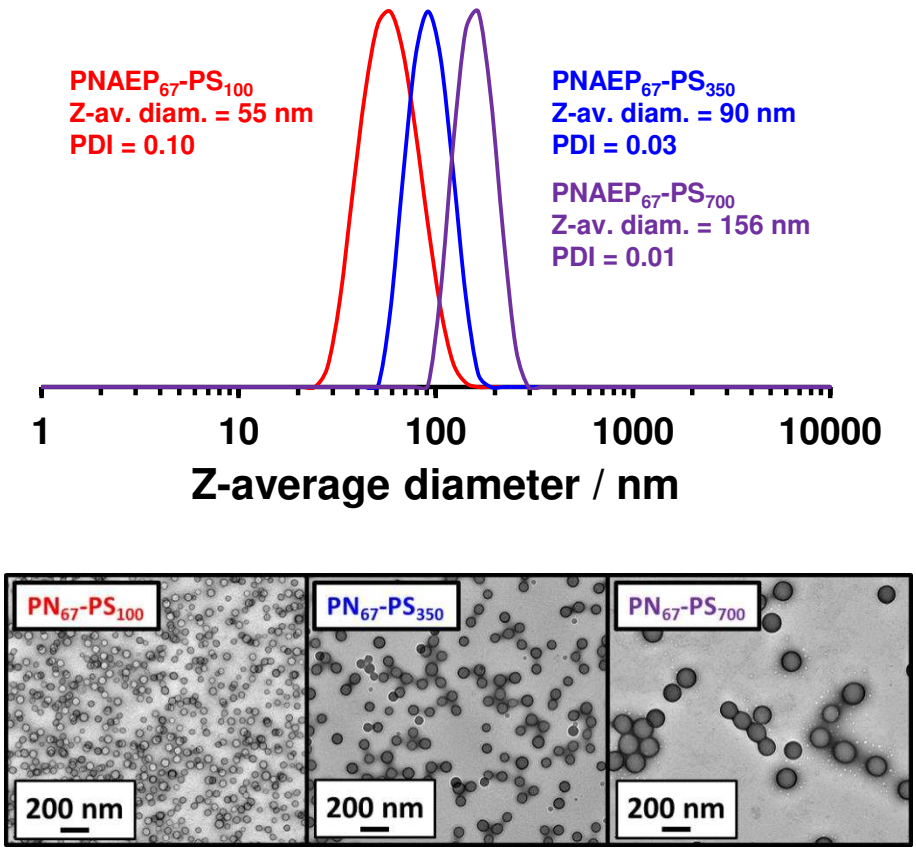

Figure 3. $PNAEP_{67}$-PS_x diblock copolymer nanoparticles prepared at 20% w/w solids *via* RAFT aqueous emulsion polymerization of styrene at 80 °C: (a) DLS particle size distributions obtained for x = 100, 350 and 700; (b) the corresponding TEM images showing well-defined kinetically-trapped spherical nanoparticles in each case.

The same $PNAEP_{67}$ was also used for the RAFT aqueous emulsion polymerization of *n*-butyl acrylate (nBA). It is well-established that acrylic polymerizations undergo chain transfer to polymer and that this side-reaction is more pronounced at higher temperatures (see Figure S5).[97-99] In view of this problem, a well-known low-temperature redox initiator couple[100-102] composed of potassium persulfate (KPS) and ascorbic acid (AsAc) was used to conduct the RAFT aqueous emulsion polymerization of nBA at 30 °C in order to minimize the degree of branching (Scheme 2).

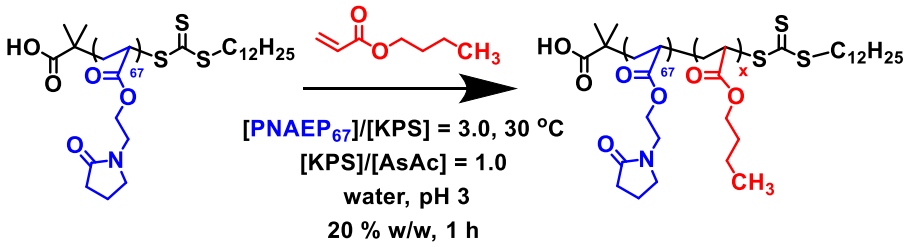

Scheme 2. Synthesis of $PNAEP_{67}$-$PnBA_x$ diblock copolymer nanoparticles *via* RAFT aqueous emulsion polymerization of *n*-butyl acrylate at 20% w/w solids using a [$PNAEP_{67}$]/[KPS] molar ratio of 3.0 and a [KPS]/[AsAc] molar ratio of 1.0. This low-temperature redox couple enables the polymerization to be conducted at 30 °C.

Representative kinetic data obtained for the RAFT aqueous emulsion polymerization of nBA at 30 °C when targeting a $PNAEP_{67}$-$PnBA_{500}$ diblock copolymer nanoparticles at 20% w/w solids is shown in Figure 4. Aliquots were taken from the polymerizing reaction solution at regular time intervals prior to analysis by ^{1}H NMR spectroscopy. The nBA polymerization proceeded after a relatively short induction period (5 min) after which an approximate 21-fold rate increase was observed, corresponding to 7% nBA conversion (Figure 4a). Moreover, visual inspection of the reaction mixture indicated that clarification of the initially milky emulsion occurred on the same time scale. DLS analysis of aliquots taken from the reaction mixture confirmed that this acceleration coincided with micellar nucleation (see Figure S1b), for which the critical PnBA DP is around 35. First-order kinetics were then observed up to 90% conversion and more than 99% nBA conversion was achieved within 25 min at 30 °C.

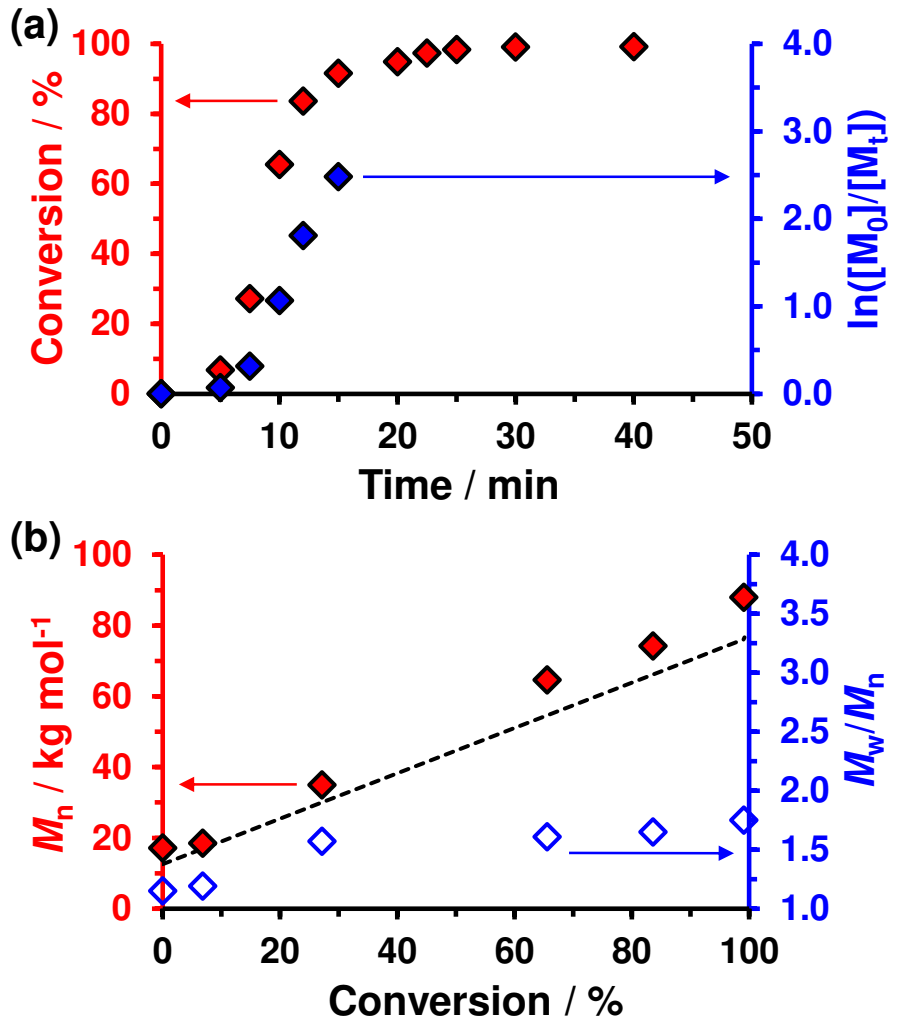

Figure 4. PISA synthesis of $PNAEP_{67}$-$PnBA_{500}$ nanoparticles at 20% w/w solids *via* RAFT aqueous emulsion polymerization of nBA at 30 °C prepared using a [$PNAEP_{67}$]/[KPS] molar ratio of 3.0: (a) conversion vs time curve and the corresponding semilogarithmic plot against time as determined by ^{1}H NMR spectroscopy; (b) evolution of M_n and M_w/M_n against conversion determined by chloroform GPC using a series of near-monodisperse polystyrene calibration standards.

Reasonable RAFT control over this polymerization was confirmed by chloroform GPC analysis, which revealed a linear relationship between M_n and monomer conversion. However, significantly broader MWDs (M_w/M_n < 1.65) were obtained compared to those observed for the styrene polymerizations, see Figure 4b. Similar observations have been reported for the RAFT aqueous emulsion polymerization of nBA by other workers.[58, 61, 98] Moreover, the experimental M_n values were

systematically higher than that expected. This can be partially attributed to the structural differences between the PNAEP-PnBA$_x$ diblock copolymers and the polystyrene standards used for GPC calibration. However, chain transfer to polymer is also likely to play a role here.[98]

Five PNAEP$_{67}$-PnBA$_x$ diblock compositions were targeted at 20% w/w solids *via* RAFT aqueous emulsion polymerization of nBA at 30°C. At least 99% conversion was achieved within 1 h when targeting PnBA DPs of up to 750, as confirmed by ^{1}H NMR spectroscopy. However, only 72% conversion was achieved when targeting a PnBA DP of 1250. Chloroform GPC analysis indicated relatively good RAFT control (M_w/M_n = 1.38) was achieved for a PnBA DP of 100 but relatively broad MWDs (M_w/M_n > 1.50) were obtained when targeting PnBA DPs above 250. Furthermore, GPC analysis confirmed that the final diblock copolymer MWDs were contaminated with 5–10% residual PNAEP$_{67}$ precursor (Figure 5). This suggests slightly lower blocking efficiencies than those achieved for the PNAEP$_{67}$-PS$_x$ nanoparticle syntheses (Figure 2).

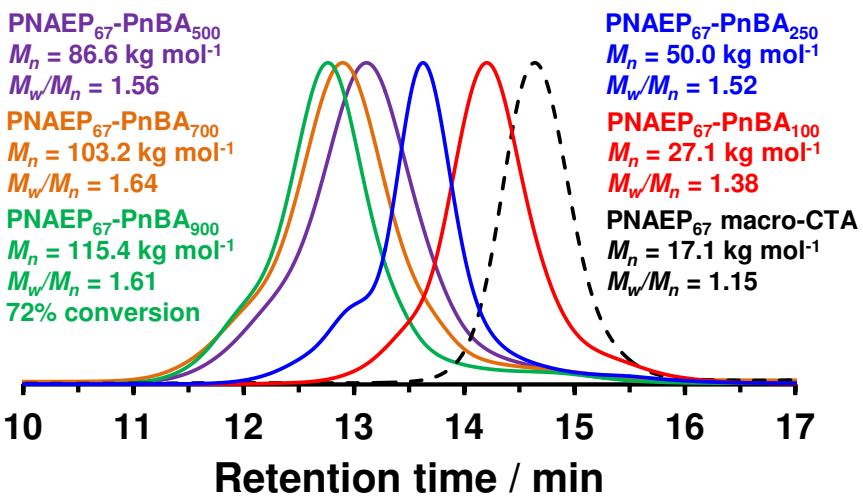

Figure 5. Chloroform GPC curves recorded for PNAEP$_{67}$-PnBA$_x$ diblock copolymers (where x = 100, 250, 500, 700 or 900) prepared at 20% w/w solids *via* RAFT aqueous emulsion polymerization of nBA at 30 °C. Molecular weight data are expressed relative to a series of near-monodisperse polystyrene calibration standards.

DLS analysis indicated that the mean sphere-equivalent nanoparticle diameter could be readily tuned from 45 nm to 141 nm simply by varying the target DP of the core-forming PnBA block from 100 to 700 for this PNAEP$_{67}$-PnBA$_x$ diblock copolymer series (Figure 6). Moreover, the relatively low DLS polydispersities are consistent with a kinetically-trapped spherical morphology. Unfortunately, the relatively low T_g of PnBA homopolymer (–54 °C)[103] precluded meaningful TEM analysis of such nanoparticles.

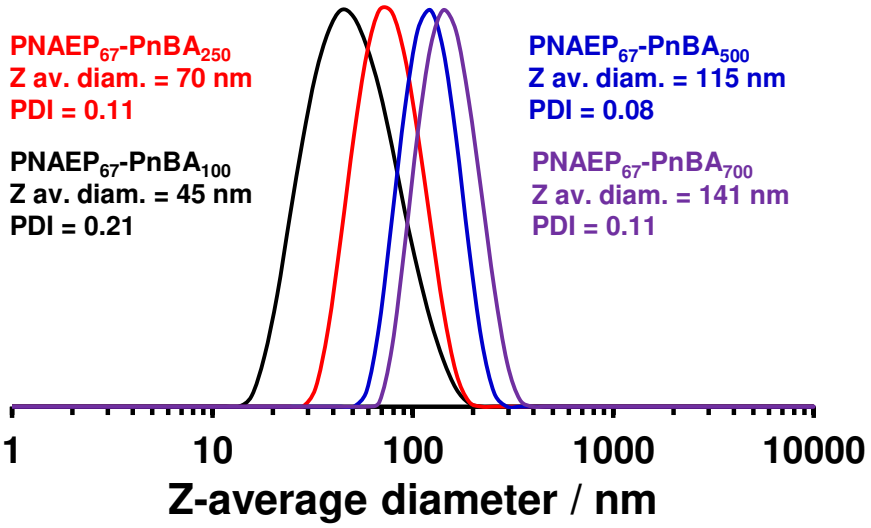

Figure 6. DLS particle size distributions recorded for four examples of PNAEP$_{67}$-PnBA$_x$ diblock copolymer nanoparticles (x = 100, 250, 500 and 700) prepared at 20% w/w solids *via* RAFT aqueous emulsion polymerization of nBA at 30 °C.

Finally, PNAEP$_{67}$-P(S-*stat*-nBA)$_x$ diblock copolymer nanoparticles were synthesized *via* RAFT emulsion statistical copolymerization of styrene (45 wt.%) with *n*-butyl acrylate (55 wt. %) at 20% w/w solids. Broad MWDs (M_w/M_n > 3.00) were observed when the synthesis of PNAEP$_{67}$-P(S-*stat*-nBA)$_x$ nanoparticles was attempted using the VA-044 initiator at 80 °C and pH 7, which correspond to the optimal conditions identified for the RAFT aqueous emulsion homopolymerization of styrene (see Figure S6). This problem is attributed to chain transfer to polymer at this relatively high reaction temperature. Moreover, some coagulum (> 15%) was also observed for such high-temperature PISA

syntheses. Thus, in order to ensure reasonable RAFT control and the formation of colloidally stable nanoparticles, the low-temperature redox initiator was utilized at pH 3, see Scheme 3.

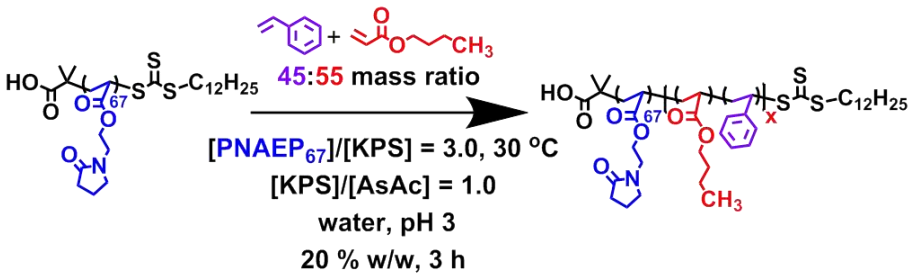

Scheme 3. Synthesis of $PNAEP_{67}$-P(S-*stat*-nBA)$_x$ diblock copolymer nanoparticles *via* RAFT aqueous emulsion statistical copolymerization of styrene with *n*-butyl acrylate at 30 °C using a [$PNAEP_{67}$]/[KPS] molar ratio of 3.0 and a [KPS]/[AsAc] molar ratio of 1.0.

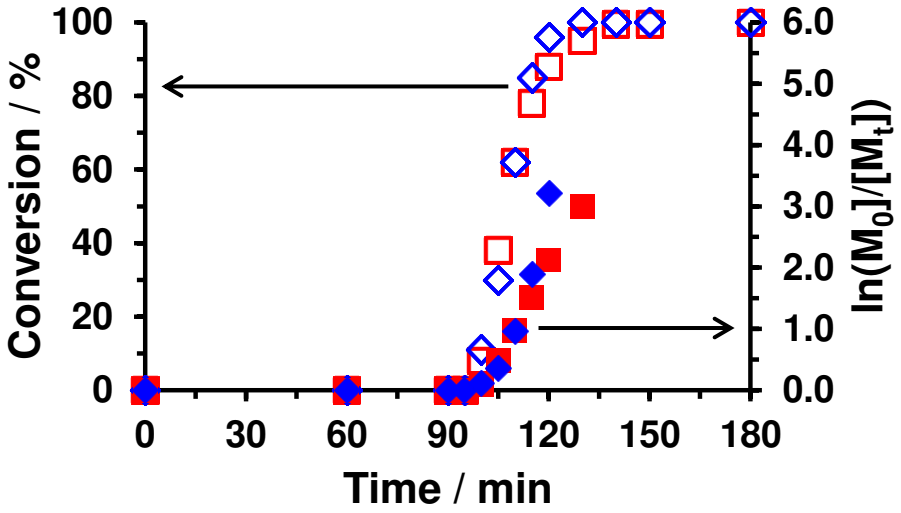

Figure 7. Conversion *vs* time curve (as determined by ^{1}H NMR spectroscopy) and the corresponding semilogarithmic plot obtained during the PISA synthesis of $PNAEP_{67}$-P(S-*stat*-nBA)$_{100}$ nanoparticles prepared at 20% w/w solids *via* RAFT aqueous emulsion statistical copolymerization of 45 wt. % styrene (red squares) with 55 wt.% nBA (blue diamonds) at 30 °C using a [$PNAEP_{67}$]/[KPS] molar ratio of 3.0.

The kinetics for the RAFT aqueous emulsion statistical copolymerization of styrene and nBA was monitored at 30 °C for a target $PNAEP_{67}$-P(S-*stat*-nBA)$_{100}$ diblock composition. Aliquots were taken

at regular time intervals and each reaction mixture was quenched by dilution and analyzed in turn using ^{1}H NMR spectroscopy (Figure 7). A much longer induction period (95 min) was observed for this copolymerization compared to those observed for the homopolymerization of styrene (10 min) or nBA (5 min) using the same $PNAEP_{67}$ precursor (see Figure 1 and Figure 4). Currently, we have no satisfactory explanation for this unexpected observation. The vinyl signals for the two comonomers were readily distinguishable by ^{1}H NMR spectroscopy, which meant that their individual rates of reaction could be monitored (see Figure S7 in the Supporting Information). After 105 min, the comonomer conversions were 11% for nBA and 8% for styrene: this is not unexpected given the significantly greater reactivity of the acrylic comonomer.[104] This time point appears to approximately correspond to the micellar nucleation event, with much greater rates of copolymerization being observed thereafter. The initial gradients were calculated for each comonomer from their corresponding semilogarithmic plots: the initial rate of copolymerization of nBA was 1.5 times faster than that of styrene. After 110 min, consumption of both comonomers had reached 62%. However, nBA was fully consumed after 130 min but only 95% styrene conversion had been achieved at this point. After 140 min, the styrene conversion reached 99%, indicating that very high final comonomer conversions can be achieved using the low-temperature redox initiator formulation.

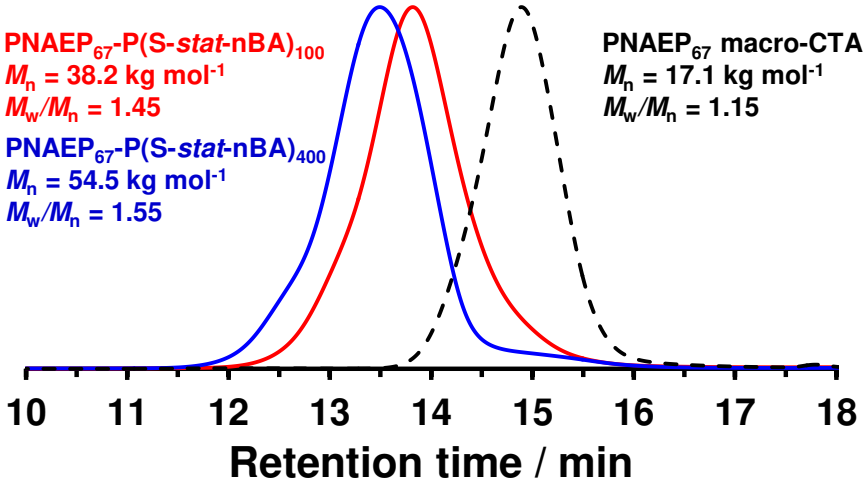

Figure 8. Chloroform GPC curves recorded for PNAEP$_{67}$-P(S-*stat*-nBA)$_x$ (where x = 100 or 400) diblock copolymer nanoparticles prepared at 20% w/w solids *via* RAFT aqueous emulsion statistical copolymerization of 45 wt.% styrene and 55 wt.% nBA at 30 °C. Molecular weight data are expressed relative to a series of near-monodisperse polystyrene calibration standards.

Two PNAEP$_{67}$-P(S-*stat*-nBA)$_x$ diblock copolymer formulations (where x = 100 or 400) were further investigated. ^{1}H NMR studies indicated that at least 99% comonomer conversion was achieved within 3 h in each case. Chloroform GPC analysis indicated that high blocking efficiencies and reasonable RAFT control (M_w/M_n < 1.55) was achieved (Figure 8). However, when an overall DP of 700 was targeted, only substantially incomplete conversions (67% and 46% conversion for nBA and styrene, respectively) were achieved under the same conditions. DLS and TEM studies on a 0.1% w/w dispersion of PNAEP$_{67}$-P(S-*stat*-nBA)$_{400}$ nanoparticles indicated kinetically-trapped spheres with a mean hydrodynamic diameter of 99 nm and a relatively narrow particle size distribution (DLS polydispersity = 0.08) were obtained (Figure 9).

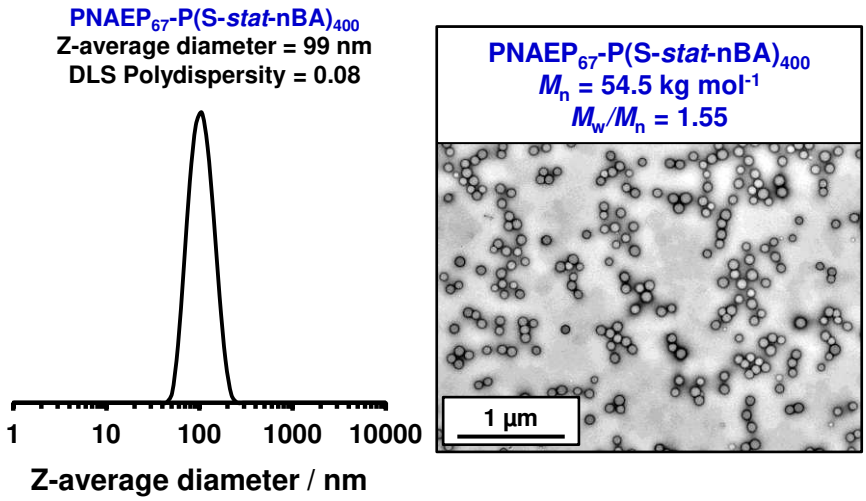

Figure 9. DLS particle size distribution and the corresponding TEM image showing well-defined kinetically-trapped PNAEP$_{67}$-P(S-*stat*-nBA)$_{400}$ spheres are formed at 20% w/w solids *via* RAFT aqueous emulsion statistical copolymerization of styrene and nBA at 30 °C.

Differential scanning calorimetry (DSC) was used to determine T_g values for the PNAEP$_{67}$-PnBA$_{100}$, PNAEP$_{67}$-P(S-*stat*-nBA)$_{100}$, PNAEP$_{67}$-P(S-*stat*-nBA)$_{400}$ and PNAEP$_{67}$-PS$_{100}$ diblock copolymers (Figure 10). Each diblock copolymer was dried from its 20 % w/w aqueous dispersion in a vacuum oven at 30 °C for at least 24 h prior to analysis. DSC studies were performed using hermetically-sealed aluminium pans at a heating rate of 10 °C min^{-1}.

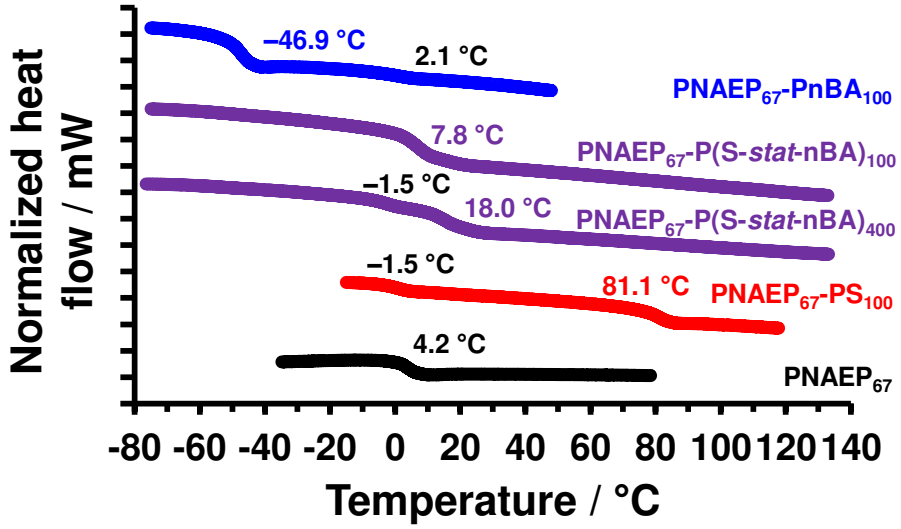

Figure 10. Differential scanning calorimetry (DSC) curves recorded at a heating rate of 10 °C min^{-1} for $PNAEP_{67}$-$PnBA_{100}$, $PNAEP_{67}$-P(S-*stat*-nBA)$_{100}$, $PNAEP_{67}$-P(S-*stat*-nBA)$_{400}$, $PNAEP_{67}$-PS_{100} and $PNAEP_{67}$ macro-CTA. DSC curves are arbitrarily offset for the sake of clarity.

DSC studies indicated that the $PNAEP_{67}$-$PnBA_{100}$ diblock copolymer had two distinct T_g values, indicating microphase separation between the hydrophilic and hydrophobic blocks (Figure 10). The lower T_g was observed at –46.9 °C which is close to that reported for PnBA homopolymer (–54 °C).[103] The second T_g occurred at 2.1 °C and is attributed to the $PNAEP_{67}$ block, because the T_g of the $PNAEP_{67}$ precursor is 4.2 °C. The DSC curve recorded for the $PNAEP_{67}$-PS_{100} diblock copolymer also exhibits two distinct T_g values at 1.3 and 81.1 °C, which correspond to the microphase-separated PNAEP and PS blocks, respectively.

According to Fox, the T_g of a statistical copolymer can be calculated using Equation 1.[105]

$$\frac{1}{T_g} = \frac{w_1}{T_{g1}} + \frac{w_2}{T_{g2}} \quad (1)$$

Where w_1 and w_2 are the weight fractions of the two comonomers and T_{g1} and T_{g2} are the T_g values for their respective homopolymers. Using the experimental T_g values for the PS_{100} and $PnBA_{100}$ blocks obtained above, the theoretical T_g of the $PNAEP_{67}$-P(S-*stat*-nBA)$_{100}$ diblock copolymer was calculated to be 9 °C. This compares well with the experimental T_g value of 7.8 °C obtained from the

corresponding DSC trace shown in Figure 10. However, the T_g of the $PNAEP_{67}$ block could not be observed because this thermal transition overlaps with that of the statistical copolymer block (Figure 10). Finally, increasing the DP from 100 to 400 raised the copolymer T_g from 7.8 to 18.0 °C, which was sufficient to enable the $PNAEP_{67}$ block T_g to be observed at approximately 1.3 °C.

The optical transparency of $PNAEP_{67}$-PS_{400}, $PNAEP_{67}$-$PnBA_{400}$ and $PNAEP_{67}$-P(S-*stat*-nBA)$_{400}$ copolymer films prepared by spin-coating the corresponding aqueous dispersions onto glass slides was initially assessed by visual inspection. Unexpectedly, spin-coating $PNAEP_{67}$-PS_{400} dispersions when targeting thin layers produced relatively good-quality films despite the high T_g of the PS component. However, increasing the film thickness led to embrittlement and a progressive reduction in transparency. Using $PNAEP_{67}$-$PnBA_{400}$ dispersions led to tacky, highly transparent films. Films prepared by spin-coating $PNAEP_{67}$-P(S-*stat*-nBA)$_{400}$ produced non-tacky, highly transparent films. Film transmittances were then assessed for three copolymer films of approximately the same mean thickness using visible absorption spectroscopy, see Figure 11.

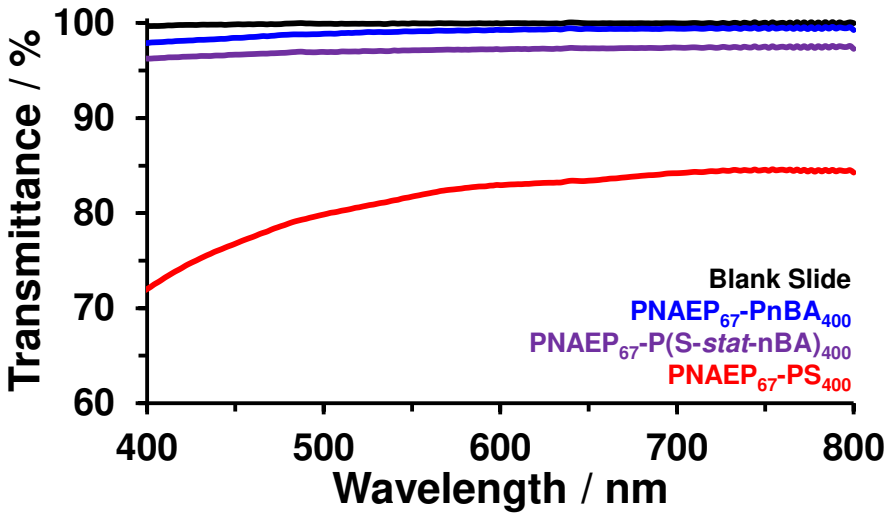

Figure 11. Transmission visible absorption spectra recorded for three copolymer films (mean film thickness = 20 µm) prepared via spin-coating 20% w/w aqueous dispersions of $PNAEP_{67}$-$PnBA_{400}$ (blue), $PNAEP_{67}$-P(S-*stat*-nBA)$_{400}$ (purple) and $PNAEP_{67}$-PS_{400} (red) nanoparticles onto glass slides at 20 °C. The transmission spectrum (black) recorded for a blank glass slide is also shown as a reference.

For 20 μm $PNAEP_{67}$-$PnBA_{400}$ and $PNAEP_{67}$-P(S-*stat*-nBA)$_{400}$ films, the transmission exceeded 95% over the entire range of wavelengths analyzed (400-800 nm) with the pure PnBA system being close to 100% transparent up to 600 nm. Conversely, films prepared from spin-coating a 20% w/w aqueous dispersion of $PNAEP_{67}$-PS_{400} diblock copolymer nanoparticles remained below 85% transmittance. The films were less transparent at shorter wavelengths, but still had a transmittance of more than 70% above 400 nm (Figure 11).

Conclusions

A trithiocarbonate-based poly(2-(*N*-acryloyloxy)ethyl pyrrolidone) macro-CTA with a degree of polymerization of 67 ($PNAEP_{67}$) was used for the RAFT emulsion polymerization of styrene, *n*-butyl acrylate and statistical mixtures thereof. RAFT emulsion polymerization of styrene using VA-044 initiator at 80 °C and pH 7 led to essentially full conversion within 40 min with induction times as short as 10 min, while GPC analysis indicated high blocking efficiency and good control over the molecular weight distribution (MWD) (M_w/M_n < 1.30). Dynamic light scattering (DLS) studies confirmed that systematically increasing the target DP from 100 to 700 enabled the z-average diameter of the resulting polystyrene-core spherical nanoparticles to be adjusted from 55 to 156 nm.

The same $PNAEP_{67}$ macro-CTA was then used for the RAFT emulsion polymerization of nBA at 30 °C using a low-temperature redox initiator at pH 3, with essentially full conversion being achieved within 25 min. High blocking efficiencies were observed up to a PnBA target DP of 700 but relatively broad MWDs (M_w/M_n < 1.64) were obtained, presumably owing to side-reactions such as chain transfer to polymer. DLS studies indicated that a series of $PNAEP_{67}$-$PnBA_x$ diblock copolymer spheres (where x = 100 to 700) exhibited z-average diameters ranging from 45 to 141 nm. Broad MWDs (M_w/M_n > 3.00) were observed when this synthesis was attempted using the VA-044 initiator at 80 °C and pH 7, which correspond to the optimal conditions identified for the RAFT aqueous emulsion homopolymerization of styrene. Moreover, coagulum (> 15%) was observed for such high-temperature PISA syntheses.

Finally, the statistical copolymerization of 45% styrene with 55% *n*-butyl acrylate was conducted with the low-temperature redox initiator at 30 °C using a $PNAEP_{67}$ macro-CTA. ^{1}H NMR analysis indicated a significantly longer induction period (95 min) compared to either homopolymerization. Nevertheless, essentially full nBA conversion was achieved after 35 min, with all the styrene monomer being consumed within 45 min. DLS and TEM studies confirmed a well-defined spherical morphology for these relatively soft nanoparticles (z-average diameter = 99 nm, DLS polydispersity = 0.08) Differential scanning calorimetry analysis indicated that these styrene/*n*-butyl acrylate copolymers exhibited intermediate glass transition temperatures compared to the two respective homopolymers. Furthermore, these experimental data were in good agreement with theoretical values calculated using the Fox equation.

The film formation behavior of selected diblock copolymer nanoparticles was explored using visible adsorption spectroscopy. $PNAEP_{67}$-PS_{400} thin layers produced relatively good-quality films despite the high T_g of the PS component. However, increasing the film thickness led to embrittlement and a reduction in transparency. $PNAEP_{67}$-$PnBA_{400}$ films were found to be tacky and highly transparent. Similarly, films prepared by spin-coating $PNAEP_{67}$-P(S-*stat*-nBA)$_{400}$ produced non-tacky, highly transparent films.

Acknowledgments

EPSRC is thanked for funding a CDT PhD studentship for the first author (EP/L016281). Ashland Specialty Ingredients (Bridgewater, New Jersey, USA) is thanked for financial support of this PhD project, for supplying the NAEP monomer and for permission to publish this work. SPA also thanks the ERC for a five-year Advanced Investigator grant (PISA 320372) and the EPSRC for an Established Career Particle Technology Fellowship (EP/R003009).

Supporting Information

Acid titration curve for an aqueous solution of HOOC-PNAEP$_{67}$ macro-CTA, hydrodynamic diameter (and DLS polydispersity) vs. pH curves obtained for PNAEP$_{67}$-PS$_{250}$ nanoparticles, TEM images obtained for a range of PNAEP$_{21}$-PS$_x$ diblock compositions and copolymer concentrations, additional GPC curves recorded for PNAEP$_{67}$-PnBA$_{500}$ and PNAEP$_{67}$-P(S-*stat*-nBA)$_{400}$ diblock copolymers, ^{1}H NMR spectra ($CDCl_3$) recorded during the synthesis of PNAEP$_{67}$-P(S-*stat*-nBA)$_{100}$ nanoparticles.

References

1. Matyjaszewski, K.; Spanswick, J. Controlled/living radical polymerization. Materials Today 2005, 8 (3), 26-33.

2. Braunecker, W. A.; Matyjaszewski, K. Controlled/living radical polymerization: Features, developments, and perspectives. Progress in Polymer Science 2007, 32 (1), 93-146.

3. Jennings, J.; He, G.; Howdle, S. M.; Zetterlund, P. B. Block copolymer synthesis by controlled/living radical polymerisation in heterogeneous systems. Chemical Society Reviews 2016, 45 (18), 5055-5084.

4. Canning, S. L.; Smith, G. N.; Armes, S. P. A Critical Appraisal of RAFT-Mediated Polymerization-Induced Self-Assembly. Macromolecules 2016, 49 (6), 1985-2001.

5. Zhou, D.; Dong, S.; Kuchel, R. P.; Perrier, S.; Zetterlund, P. B. Polymerization induced self-assembly: tuning of morphology using ionic strength and pH. Polymer Chemistry 2017, 8 (20), 3082-3089.

6. Blanazs, A.; Madsen, J.; Battaglia, G.; Ryan, A. J.; Armes, S. P. Mechanistic Insights for Block Copolymer Morphologies: How Do Worms Form Vesicles? Journal of the American Chemical Society 2011, 133 (41), 16581-16587.

7. Zehm, D.; Ratcliffe, L. P. D.; Armes, S. P. Synthesis of Diblock Copolymer Nanoparticles via RAFT Alcoholic Dispersion Polymerization: Effect of Block Copolymer Composition, Molecular Weight, Copolymer Concentration, and Solvent Type on the Final Particle Morphology. Macromolecules 2013, 46 (1), 128-139.

8. Lansalot, M.; Rieger, J. Polymerization-Induced Self-Assembly. Macromolecular Rapid Communications 2019, 40 (2), 1800885.

9. Charleux, B.; Delaittre, G.; Rieger, J.; D'Agosto, F. Polymerization-Induced Self-Assembly: From Soluble Macromolecules to Block Copolymer Nano-Objects in One Step. Macromolecules 2012, 45 (17), 6753-6765.

10. Binauld, S.; Delafresnaye, L.; Charleux, B.; D'Agosto, F.; Lansalot, M. Emulsion Polymerization of Vinyl Acetate in the Presence of Different Hydrophilic Polymers Obtained by RAFT/MADIX. Macromolecules 2014, 47 (10), 3461-3472.

11. Zhao, W.; Gody, G.; Dong, S.; Zetterlund, P. B.; Perrier, S. Optimization of the RAFT polymerization conditions for the in situ formation of nano-objects via dispersion polymerization in alcoholic medium. Polymer Chemistry 2014, 5 (24), 6990-7003.

12. Blackman, L. D.; Doncom, K. E. B.; Gibson, M. I.; O'Reilly, R. K. Comparison of photo- and thermally initiated polymerization-induced self-assembly: a lack of end group fidelity drives the formation of higher order morphologies. Polymer Chemistry 2017, 8 (18), 2860-2871.

13. Foster, J. C.; Varlas, S.; Couturaud, B.; Jones, J. R.; Keogh, R.; Mathers, R. T.; O'Reilly, R. K. Predicting Monomers for Use in Polymerization-Induced Self-Assembly. Angewandte Chemie International Edition 2018, 57 (48), 15733-15737.

14. Zhou, D.; Kuchel, R. P.; Dong, S.; Lucien, F. P.; Perrier, S.; Zetterlund, P. B. Polymerization-Induced Self-Assembly under Compressed CO2: Control of Morphology Using a CO2-Responsive MacroRAFT Agent. Macromolecular Rapid Communications 2019, 40 (2), 1800335.

15. Wang, X.; An, Z. New Insights into RAFT Dispersion Polymerization-Induced Self-Assembly: From Monomer Library, Morphological Control, and Stability to Driving Forces. Macromolecular Rapid Communications 2019, 40 (2), 1800325.

16. Zhang, B.; Lv, X.; An, Z. Modular Monomers with Tunable Solubility: Synthesis of Highly Incompatible Block Copolymer Nano-Objects via RAFT Aqueous Dispersion Polymerization. ACS Macro Letters 2017, 6 (3), 224-228.

17. Zhang, L.; Eisenberg, A. Multiple Morphologies of "Crew-Cut" Aggregates of Polystyrene-b-poly(acrylic acid) Block Copolymers. Science 1995, 268 (5218), 1728.

18. Discher, D. E.; Eisenberg, A. Polymer Vesicles. Science 2002, 297 (5583), 967.

19. Jain, S.; Bates, F. S. On the Origins of Morphological Complexity in Block Copolymer Surfactants. Science 2003, 300 (5618), 460.

20. Warren, N. J.; Armes, S. P. Polymerization-Induced Self-Assembly of Block Copolymer Nano-objects via RAFT Aqueous Dispersion Polymerization. Journal of the American Chemical Society 2014, 136 (29), 10174-10185.

21. Moad, G.; Rizzardo, E.; Thang, S. H. Living Radical Polymerization by the RAFT Process A Second Update. Australian Journal of Chemistry 2009, 62 (11), 1402-1472.

22. Moad, G.; Rizzardo, E.; Thang, S. H. Living Radical Polymerization by the RAFT ProcessA First Update. Australian Journal of Chemistry 2006, 59 (10), 669-692.

23. Moad, G.; Rizzardo, E.; Thang, S. H. Radical addition–fragmentation chemistry in polymer synthesis. Polymer 2008, 49 (5), 1079-1131.

24. Moad, G. RAFT polymerization to form stimuli-responsive polymers. Polymer Chemistry 2017, 8 (1), 177-219.

25. Matyjaszewski, K. Atom Transfer Radical Polymerization (ATRP): Current Status and Future Perspectives. Macromolecules 2012, 45 (10), 4015-4039.

26. Nicolas, J.; Guillaneuf, Y.; Lefay, C.; Bertin, D.; Gigmes, D.; Charleux, B. Nitroxide-mediated polymerization. Progress in Polymer Science 2013, 38 (1), 63-235.

27. Varlas, S.; Georgiou, P. G.; Bilalis, P.; Jones, J. R.; Hadjichristidis, N.; O'Reilly, R. K. Poly(sarcosine)-Based Nano-Objects with Multi-Protease Resistance by Aqueous Photoinitiated Polymerization-Induced Self-Assembly (Photo-PISA). Biomacromolecules 2018, 19 (11), 4453-4462.

28. Li, Z.; Zhang, Y.; Wu, L.; Yu, W.; Wilks, T. R.; Dove, A. P.; Ding, H.-M.; O'Reilly, R. K.; Chen, G.; Jiang, M. Glyco-Platelets with Controlled Morphologies via Crystallization-Driven Self-Assembly and Their Shape-Dependent Interplay with Macrophages. ACS Macro Letters 2019, 8 (5), 596-602.

29. Carlsson, L.; Fall, A.; Chaduc, I.; Wågberg, L.; Charleux, B.; Malmström, E.; D'Agosto, F.; Lansalot, M.; Carlmark, A. Modification of cellulose model surfaces by cationic polymer latexes prepared by RAFT-mediated surfactant-free emulsion polymerization. Polymer Chemistry 2014, 5 (20), 6076-6086.

30. St Thomas, C.; Guerrero-Santos, R.; D'Agosto, F. Alkoxyamine-functionalized latex nanoparticles through RAFT polymerization-induced self-assembly in water. Polymer Chemistry 2015, 6 (30), 5405-5413.

31. Chaduc, I.; Reynaud, E.; Dumas, L.; Albertin, L.; D'Agosto, F.; Lansalot, M. From well-defined poly(N-acryloylmorpholine)-stabilized nanospheres to uniform mannuronan- and guluronan-decorated nanoparticles by RAFT polymerization-induced self-assembly. Polymer 2016, 106, 218-228.

32. Karagoz, B.; Esser, L.; Duong, H. T.; Basuki, J. S.; Boyer, C.; Davis, T. P. Polymerization-Induced Self-Assembly (PISA) – control over the morphology of nanoparticles for drug delivery applications. Polymer Chemistry 2014, 5 (2), 350-355.

33. Truong, N. P.; Zhang, C.; Nguyen, T. A. H.; Anastasaki, A.; Schulze, M. W.; Quinn, J. F.; Whittaker, A. K.; Hawker, C. J.; Whittaker, M. R.; Davis, T. P. Overcoming Surfactant-Induced Morphology Instability of Noncrosslinked Diblock Copolymer Nano-Objects Obtained by RAFT Emulsion Polymerization. ACS Macro Letters 2018, 7 (2), 159-165.

34. Grazon, C.; Rieger, J.; Méallet-Renault, R.; Charleux, B.; Clavier, G. Ultrabright Fluorescent Polymeric Nanoparticles Made from a New Family of BODIPY Monomers. Macromolecules 2013, 46 (13), 5167-5176.

35. Tan, J.; Sun, H.; Yu, M.; Sumerlin, B. S.; Zhang, L. Photo-PISA: Shedding Light on Polymerization-Induced Self-Assembly. ACS Macro Letters 2015, 4 (11), 1249-1253.

36. Figg, C. A.; Carmean, R. N.; Bentz, K. C.; Mukherjee, S.; Savin, D. A.; Sumerlin, B. S. Tuning Hydrophobicity To Program Block Copolymer Assemblies from the Inside Out. Macromolecules 2017, 50 (3), 935-943.

37. Derry, M. J.; Fielding, L. A.; Armes, S. P. Polymerization-induced self-assembly of block copolymer nanoparticles via RAFT non-aqueous dispersion polymerization. Progress in Polymer Science 2016, 52, 1-18.

38. Semsarilar, M.; Jones, E. R.; Blanazs, A.; Armes, S. P. Efficient Synthesis of Sterically-Stabilized Nano-Objects via RAFT Dispersion Polymerization of Benzyl Methacrylate in Alcoholic Media. Advanced Materials 2012, 24 (25), 3378-3382.

39. Jones, E. R.; Mykhaylyk, O. O.; Semsarilar, M.; Boerakker, M.; Wyman, P.; Armes, S. P. How Do Spherical Diblock Copolymer Nanoparticles Grow during RAFT Alcoholic Dispersion Polymerization? Macromolecules 2016, 49 (1), 172-181.

40. Ma, Y.; Gao, P.; Ding, Y.; Huang, L.; Wang, L.; Lu, X.; Cai, Y. Visible Light Initiated Thermoresponsive Aqueous Dispersion Polymerization-Induced Self-Assembly. Macromolecules 2019, 52 (3), 1033-1041.

41. Warren, N. J.; Derry, M. J.; Mykhaylyk, O. O.; Lovett, J. R.; Ratcliffe, L. P. D.; Ladmiral, V.; Blanazs, A.; Fielding, L. A.; Armes, S. P. Critical Dependence of Molecular Weight on Thermoresponsive Behavior of Diblock Copolymer Worm Gels in Aqueous Solution. Macromolecules 2018, 51 (21), 8357-8371.

42. Martín-Fabiani, I.; Lesage de la Haye, J.; Schulz, M.; Liu, Y.; Lee, M.; Duffy, B.; D'Agosto, F.; Lansalot, M.; Keddie, J. L. Enhanced Water Barrier Properties of Surfactant-Free Polymer Films Obtained by MacroRAFT-Mediated Emulsion Polymerization. ACS Applied Materials & Interfaces 2018, 10 (13), 11221-11232.

43. Lesage de la Haye, J.; Martin-Fabiani, I.; Schulz, M.; Keddie, J. L.; D'Agosto, F.; Lansalot, M. Hydrophilic MacroRAFT-Mediated Emulsion Polymerization: Synthesis of Latexes for Cross-Linked and Surfactant-Free Films. Macromolecules 2017, 50 (23), 9315-9328.

44. Cockram, A. A.; Bradley, R. D.; Lynch, S. A.; Fleming, P. C. D.; Williams, N. S. J.; Murray, M. W.; Emmett, S. N.; Armes, S. P. Optimization of the high-throughput synthesis of multiblock copolymer nanoparticles in aqueous media via polymerization-induced self-assembly. Reaction Chemistry & Engineering 2018, 3 (5), 645-657.

45. Tan, J.; Dai, X.; Zhang, Y.; Yu, L.; Sun, H.; Zhang, L. Photoinitiated Polymerization-Induced Self-Assembly via Visible Light-Induced RAFT-Mediated Emulsion Polymerization. ACS Macro Letters 2019, 8 (2), 205-212.

46. Khor, S. Y.; Truong, N. P.; Quinn, J. F.; Whittaker, M. R.; Davis, T. P. Polymerization-Induced Self-Assembly: The Effect of End Group and Initiator Concentration on Morphology of Nanoparticles Prepared via RAFT Aqueous Emulsion Polymerization. ACS Macro Letters 2017, 6 (9), 1013-1019.

47. Ratcliffe, L. P. D.; Blanazs, A.; Williams, C. N.; Brown, S. L.; Armes, S. P. RAFT polymerization of hydroxy-functional methacrylic monomers under heterogeneous conditions: effect of varying the core-forming block. Polymer Chemistry 2014, 5 (11), 3643-3655.

48. Zhou, J.; Yao, H.; Ma, J. Recent advances in RAFT-mediated surfactant-free emulsion polymerization. Polymer Chemistry 2018, 9 (19), 2532-2561.

49. Truong, N. P.; Quinn, J. F.; Anastasaki, A.; Rolland, M.; Vu, M. N.; Haddleton, D. M.; Whittaker, M. R.; Davis, T. P. Surfactant-free RAFT emulsion polymerization using a novel biocompatible thermoresponsive polymer. Polymer Chemistry 2017, 8 (8), 1353-1363.

50. Martín-Fabiani, I.; Makepeace, D. K.; Richardson, P. G.; Lesage de la Haye, J.; Venero, D. A.; Rogers, S. E.; D'Agosto, F.; Lansalot, M.; Keddie, J. L. In Situ Monitoring of Latex Film Formation by Small-Angle Neutron Scattering: Evolving Distributions of Hydrophilic Stabilizers in Drying Colloidal Films. Langmuir 2019, 35 (10), 3822-3831.

51. Guyot, A. Polymerizable surfactants. Current Opinion in Colloid & Interface Science 1996, 1 (5), 580-586.

52. Zhang, X.; Boisson, F.; Colombani, O.; Chassenieux, C.; Charleux, B. Synthesis of Amphiphilic Poly(acrylic acid)-b-poly(n-butyl acrylate-co-acrylic acid) Block Copolymers with Various Microstructures via RAFT Polymerization in Water/Ethanol Heterogeneous Media. Macromolecules 2014, 47 (1), 51-60.

53. Chaduc, I.; Girod, M.; Antoine, R.; Charleux, B.; D'Agosto, F.; Lansalot, M. Batch Emulsion Polymerization Mediated by Poly(methacrylic acid) MacroRAFT Agents: One-Pot Synthesis of Self-Stabilized Particles. Macromolecules 2012, 45 (15), 5881-5893.

54. Zhang, W.; D'Agosto, F.; Dugas, P.-Y.; Rieger, J.; Charleux, B. RAFT-mediated one-pot aqueous emulsion polymerization of methyl methacrylate in presence of poly(methacrylic acid-co-poly(ethylene oxide) methacrylate) trithiocarbonate macromolecular chain transfer agent. Polymer 2013, 54 (8), 2011-2019.

55. Chaduc, I.; Crepet, A.; Boyron, O.; Charleux, B.; D'Agosto, F.; Lansalot, M. Effect of the pH on the RAFT Polymerization of Acrylic Acid in Water. Application to the Synthesis of Poly(acrylic acid)-

Stabilized Polystyrene Particles by RAFT Emulsion Polymerization. Macromolecules 2013, 46 (15), 6013-6023.

56. Cunningham, V. J.; Alswieleh, A. M.; Thompson, K. L.; Williams, M.; Leggett, G. J.; Armes, S. P.; Musa, O. M. Poly(glycerol monomethacrylate)–Poly(benzyl methacrylate) Diblock Copolymer Nanoparticles via RAFT Emulsion Polymerization: Synthesis, Characterization, and Interfacial Activity. Macromolecules 2014, 47 (16), 5613-5623.

57. Akpinar, B.; Fielding, L. A.; Cunningham, V. J.; Ning, Y.; Mykhaylyk, O. O.; Fowler, P. W.; Armes, S. P. Determining the Effective Density and Stabilizer Layer Thickness of Sterically Stabilized Nanoparticles. Macromolecules 2016, 49 (14), 5160-5171.

58. Gurnani, P.; Sanchez-Cano, C.; Abraham, K.; Xandri-Monje, H.; Cook, A. B.; Hartlieb, M.; Lévi, F.; Dallmann, R.; Perrier, S. RAFT Emulsion Polymerization as a Platform to Generate Well-Defined Biocompatible Latex Nanoparticles. Macromolecular Bioscience 2018, 18 (10), 1800213.

59. Hatton, F. L.; Park, A. M.; Zhang, Y.; Fuchs, G. D.; Ober, C. K.; Armes, S. P. Aqueous one-pot synthesis of epoxy-functional diblock copolymer worms from a single monomer: new anisotropic scaffolds for potential charge storage applications. Polymer Chemistry 2019, 10 (2), 194-200.

60. Jesson, C. P.; Cunningham, V. J.; Smallridge, M. J.; Armes, S. P. Synthesis of High Molecular Weight Poly(glycerol monomethacrylate) via RAFT Emulsion Polymerization of Isopropylideneglycerol Methacrylate. Macromolecules 2018, 51 (9), 3221-3232.

61. Rieger, J.; Osterwinter, G.; Bui, C.; Stoffelbach, F.; Charleux, B. Surfactant-Free Controlled/Living Radical Emulsion (Co)polymerization of n-Butyl Acrylate and Methyl Methacrylate via RAFT Using Amphiphilic Poly(ethylene oxide)-Based Trithiocarbonate Chain Transfer Agents. Macromolecules 2009, 42 (15), 5518-5525.

62. Xu, J.; Xiao, X.; Zhang, Y.; Zhang, W.; Sun, P. RAFT-mediated emulsion polymerization of styrene using brush copolymer as surfactant macro-RAFT agent: Effect of the brush copolymer

sequence and chemical composition. Journal of Polymer Science Part A: Polymer Chemistry 2013, 51 (5), 1147-1161.

63. Truong, N. P.; Dussert, M. V.; Whittaker, M. R.; Quinn, J. F.; Davis, T. P. Rapid synthesis of ultrahigh molecular weight and low polydispersity polystyrene diblock copolymers by RAFT-mediated emulsion polymerization. Polymer Chemistry 2015, 6 (20), 3865-3874.

64. Teodorescu, M.; Bercea, M. Poly(vinylpyrrolidone) – A Versatile Polymer for Biomedical and Beyond Medical Applications. Polymer-Plastics Technology and Engineering 2015, 54 (9), 923-943.

65. Haaf, F.; Sanner, A.; Straub, F. Polymers of N-Vinylpyrrolidone: Synthesis, Characterization and Uses. Polymer Journal 1985, 17, 143.

66. Jiang, J.; Zhu, L.; Zhu, L.; Zhang, H.; Zhu, B.; Xu, Y. Antifouling and Antimicrobial Polymer Membranes Based on Bioinspired Polydopamine and Strong Hydrogen-Bonded Poly(N-vinyl pyrrolidone). ACS Applied Materials & Interfaces 2013, 5 (24), 12895-12904.

67. Prosapio, V.; Reverchon, E.; De Marco, I. Coprecipitation of Polyvinylpyrrolidone/β-Carotene by Supercritical Antisolvent Processing. Industrial & Engineering Chemistry Research 2015, 54 (46), 11568-11575.

68. Bergemann, U.; Schmarje, S. Polymer combination from at least two different n-vinylpyrrolidone/n-vinylcaprolactam copolymers for cosmetic hair shine products. WO2010127923A3, 2012.

69. John, V. K. Hair care preparations containing N-vinyl pyrrolidone homo- and copolymers and a quaternized copolymer of vinyl pyrrolidone. US3914403, 1975.

70. Guinaudeau, A.; Mazieres, S.; Wilson, D. J.; Destarac, M. Aqueous RAFT/MADIX polymerisation of N-vinyl pyrrolidone at ambient temperature. Polymer Chemistry 2012, 3 (1), 81-84.

71. Nguyen, T. L. U.; Eagles, K.; Davis, T. P.; Barner-Kowollik, C.; Stenzel, M. H. Investigation of the influence of the architectures of poly(vinyl pyrrolidone) polymers made via the reversible addition–fragmentation chain transfer/macromolecular design via the interchange of xanthates mechanism on the stabilization of suspension polymerizations. Journal of Polymer Science Part A: Polymer Chemistry 2006, 44 (15), 4372-4383.

72. Wan, D.; Satoh, K.; Kamigaito, M.; Okamoto, Y. Xanthate-Mediated Radical Polymerization of N-Vinylpyrrolidone in Fluoroalcohols for Simultaneous Control of Molecular Weight and Tacticity. Macromolecules 2005, 38 (25), 10397-10405.

73. Roka, N.; Pitsikalis, M. Statistical copolymers of N-vinylpyrrolidone and benzyl methacrylate via RAFT: Monomer reactivity ratios, thermal properties and kinetics of thermal decomposition. Journal of Macromolecular Science, Part A 2018, 55 (3), 222-230.

74. Pound, G.; Eksteen, Z.; Pfukwa, R.; McKenzie, J. M.; Lange, R. F. M.; Klumperman, B. Unexpected reactions associated with the xanthate-mediated polymerization of N-vinylpyrrolidone. Journal of Polymer Science Part A: Polymer Chemistry 2008, 46 (19), 6575-6593.

75. Guinaudeau, A.; Coutelier, O.; Sandeau, A.; Mazières, S.; Nguyen Thi, H. D.; Le Drogo, V.; Wilson, D. J.; Destarac, M. Facile Access to Poly(N-vinylpyrrolidone)-Based Double Hydrophilic Block Copolymers by Aqueous Ambient RAFT/MADIX Polymerization. Macromolecules 2014, 47 (1), 41-50.

76. Pound, G.; McKenzie, J. M.; Lange, R. F. M.; Klumperman, B. Polymer-protein conjugates from [small omega]-aldehyde endfunctional poly(N-vinylpyrrolidone) synthesised via xanthate-mediated living radical polymerisation. Chemical Communications 2008, (27), 3193-3195.

77. Destarac, M.; Wilson, J. Stabilisants réactifs poly(N-vinyl lactame) vivants pour polymérisation en phase dispersée. WO2013/113750, 2013.

78. Cunningham, V. J.; Ning, Y.; Armes, S. P.; Musa, O. M. Poly(N-2-(methacryloyloxy)ethyl pyrrolidone)-poly(benzyl methacrylate) diblock copolymer nano-objects via RAFT alcoholic dispersion polymerisation in ethanol. Polymer 2016, 106, 189-199.

79. Cunningham, V. J.; Armes, S. P.; Musa, O. M. Synthesis, characterisation and Pickering emulsifier performance of poly(stearyl methacrylate)-poly(N-2-(methacryloyloxy)ethyl pyrrolidone) diblock copolymer nano-objects via RAFT dispersion polymerisation in n-dodecane. Polymer Chemistry 2016, 7 (10), 1882-1891.

80. Cunningham, V. J.; Derry, M. J.; Fielding, L. A.; Musa, O. M.; Armes, S. P. RAFT Aqueous Dispersion Polymerization of N-(2-(Methacryloyloxy)ethyl)pyrrolidone: A Convenient Low Viscosity Route to High Molecular Weight Water-Soluble Copolymers. Macromolecules 2016, 49 (12), 4520-4533.

81. Gibson, R. R.; Armes, S. P.; Musa, O. M.; Fernyhough, A. End-group ionisation enables the use of poly(N-(2-methacryloyloxy)ethyl pyrrolidone) as an electrosteric stabiliser block for polymerisation-induced self-assembly in aqueous media. Polymer Chemistry 2019, 10 (11), 1312-1323.

82. Shi, Y.; Liu, G.; Gao, H.; Lu, L.; Cai, Y. Effect of Mild Visible Light on Rapid Aqueous RAFT Polymerization of Water-Soluble Acrylic Monomers at Ambient Temperature: Initiation and Activation. Macromolecules 2009, 42 (12), 3917-3926.

83. Deane, O. J.; Lovett, J. R.; Musa, O. M.; Fernyhough, A.; Armes, S. P. Synthesis of Well-Defined Pyrrolidone-Based Homopolymers and Stimulus-Responsive Diblock Copolymers via RAFT Aqueous Solution Polymerization of 2-(N-Acryloyloxy)ethylpyrrolidone. Macromolecules 2018, 51 (19), 7756-7766.

84. Pham, B. T. T.; Nguyen, D.; Huynh, V. T.; Pan, E. H.; Shirodkar-Robinson, B.; Carey, M.; Serelis, A. K.; Warr, G. G.; Davey, T.; Such, C. H.; Hawkett, B. S. Aqueous Polymeric Hollow Particles as an

Opacifier by Emulsion Polymerization Using Macro-RAFT Amphiphiles. Langmuir 2018, 34 (14), 4255-4263.

85. Zhang, W.-J.; Hong, C.-Y.; Pan, C.-Y. Fabrication and characterization of silica nanotubes with controlled dimensions. Journal of Materials Chemistry A 2014, 2 (21), 7819-7828.

86. Zhang, W.; D'Agosto, F.; Boyron, O.; Rieger, J.; Charleux, B. Toward a Better Understanding of the Parameters that Lead to the Formation of Nonspherical Polystyrene Particles via RAFT-Mediated One-Pot Aqueous Emulsion Polymerization. Macromolecules 2012, 45 (10), 4075-4084.

87. Chenal, M.; Véchambre, C.; Chenal, J.-M.; Chazeau, L.; Humblot, V.; Bouteiller, L.; Creton, C.; Rieger, J. Mechanical properties of nanostructured films with an ultralow volume fraction of hard phase. Polymer 2017, 109, 187-196.

88. Carrot, G.; Diamanti, S.; Manuszak, M.; Charleux, B.; Vairon, J.-P. Atom transfer radical polymerization of n-butyl acrylate from silica nanoparticles. Journal of Polymer Science Part A: Polymer Chemistry 2001, 39 (24), 4294-4301.

89. Kan, C. Y.; Liu, D. S.; Kong, X. Z.; Zhu, X. L. Study on the preparation and properties of styrene–butyl acrylate–silicone copolymer latices. Journal of Applied Polymer Science 2001, 82 (13), 3194-3200.

90. Lu, Y.; Xia, Y.; Larock, R. C. Surfactant-free core–shell hybrid latexes from soybean oil-based waterborne polyurethanes and poly(styrene-butyl acrylate). Progress in Organic Coatings 2011, 71 (4), 336-342.

91. Stoffelbach, F.; Tibiletti, L.; Rieger, J.; Charleux, B. Surfactant-Free, Controlled/Living Radical Emulsion Polymerization in Batch Conditions Using a Low Molar Mass, Surface-Active Reversible Addition-Fragmentation Chain-Transfer (RAFT) Agent. Macromolecules 2008, 41 (21), 7850-7856.

92. Bernard, J.; Save, M.; Arathoon, B.; Charleux, B. Preparation of a xanthate-terminated dextran by click chemistry: Application to the synthesis of polysaccharide-coated nanoparticles via surfactant-

free ab initio emulsion polymerization of vinyl acetate. Journal of Polymer Science Part A: Polymer Chemistry 2008, 46 (8), 2845-2857.

93. Lane, W. H. Determination of Solubility of Styrene in Water and of Water in Styrene. Industrial & Engineering Chemistry Analytical Edition 1946, 18 (5), 295-296.

94. Mai, Y.; Eisenberg, A. Self-assembly of block copolymers. Chemical Society Reviews 2012, 41 (18), 5969-5985.

95. Brotherton, E. E.; Hatton, F. L.; Cockram, A. A.; Derry, M. J.; Czajka, A.; Cornel, E. J.; Topham, P. D.; Mykhaylyk, O. O.; Armes, S. P. In Situ Small-Angle X-ray Scattering Studies During Reversible Addition–Fragmentation Chain Transfer Aqueous Emulsion Polymerization. Journal of the American Chemical Society 2019, 141 (34), 13664-13675.

96. Lesage de la Haye, J.; Zhang, X.; Chaduc, I.; Brunel, F.; Lansalot, M.; D'Agosto, F. The Effect of Hydrophile Topology in RAFT-Mediated Polymerization-Induced Self-Assembly. Angewandte Chemie International Edition 2016, 55 (11), 3739-3743.

97. Agirre, A.; Santos, J. I.; Etxeberria, A.; Sauerland, V.; Leiza, J. R. Polymerization of n-butyl acrylate with high concentration of a chain transfer agent (CBr4): detailed characterization and impact on branching. Polymer Chemistry 2013, 4 (6), 2062-2079.

98. Ahmad, N. M.; Charleux, B.; Farcet, C.; Ferguson, C. J.; Gaynor, S. G.; Hawkett, B. S.; Heatley, F.; Klumperman, B.; Konkolewicz, D.; Lovell, P. A.; Matyjaszewski, K.; Venkatesh, R. Chain Transfer to Polymer and Branching in Controlled Radical Polymerizations of n-Butyl Acrylate. Macromolecular Rapid Communications 2009, 30 (23), 2002-2021.

99. Johnson, I. J.; Khosravi, E.; Musa, O. M.; Simnett, R. E.; Eissa, A. M. Xanthates designed for the preparation of N-Vinyl pyrrolidone-based linear and star architectures via RAFT polymerization. Journal of Polymer Science Part A: Polymer Chemistry 2015, 53 (6), 775-786.

100. Misra, G. S.; Gupta, C. V. Aqueous polymerization of methacrylamide initiated by the redox system K2S2O8/ascorbic acid. Die Makromolekulare Chemie 1973, 165 (1), 205-216.

101. Narain, H.; Jagadale, S. M.; Ghatge, N. D. Studies of redox polymerization. I. Aqueous polymerization of acrylamide by an ascorbic acid–peroxydisulfate system. Journal of Polymer Science: Polymer Chemistry Edition 1981, 19 (5), 1225-1238.

102. Cabelli, D. E.; Bielski, B. H. J. Kinetics and mechanism for the oxidation of ascorbic acid/ascorbate by HO2/O2- (hydroperoxyl/superoxide) radicals. A pulse radiolysis and stopped-flow photolysis study. The Journal of Physical Chemistry 1983, 87 (10), 1809-1812.

103. Wiley, R. H.; Brauer, G. M. Refractometric determination of second-order transition temperatures in polymers. III. Acrylates and methacrylates. Journal of Polymer Science 1948, 3 (5), 647-651.

104. Lyons, R. A.; Hutovic, J.; Piton, M. C.; Christie, D. I.; Clay, P. A.; Manders, B. G.; Kable, S. H.; Gilbert, R. G. Pulsed-Laser Polymerization Measurements of the Propagation Rate Coefficient for Butyl Acrylate. Macromolecules 1996, 29 (6), 1918-1927.

105. Fox, T. G. Influence of Diluent and of Copolymer Composition on the Glass Temperature of a Poly-mer System. Bull. Am. Phys. Soc. 1956, 1, 123.